A Fast Multi-Objective Optimization Approach to S-Duct Scoop Inlets Design with Both Inflow and Outflow

Lifang Zeng, Dingyi Pan*, Shangjun Ye, Xueming Shao

Abstract

A fast multi-objective optimization method for S-duct scoop inlets considering both inflow and outflow is developed and validated. To reduce computation consumption of optimization, a simplified efficient model is proposed, in which only inflow region is simulated. Inlet pressure boundary condition of the efficient model is specified by solving an integral model with both inflow and outflow. An automated optimization system integrating the computational fluid dynamics (CFD) analysis, Non-Uniform Rational B-Spline (NURBS) geometric representation technique, Non-dominated Sorting Genetic Algorithm II (NSGA-II) is developed to minimize total pressure loss and distortion at the exit of diffuser. Flow field is numerically simulated by solving the Reynolds Average Navier-Stokes equation coupled with k–ω Shear Stress Transport (SST) turbulence model, and results are validated to agree well with previous experiment. S-duct centreline shape and cross-section area distribution are parameterized as the design variables. By analysing the results of a suggested optimal inlet chosen from the obtained Pareto Front, total pressure recovery has increased from 97% to 97.4%, and total pressure distortion *DC60* has decreased by 0.0477 (21.7% of origin) at designed Mach number 0.7. The simplified efficient model has been validated to be reliable, and by which the time cost for the optimization project has been reduced by 70%.

Keywords

S-Duct Inlets, Multi-Objective Optimization, efficient model, integral model, total pressure recovery, total pressure distortion, outer flow

School of Aeronautics and Astronautics, Zhejiang University, Hangzhou 310027, China

*Corresponding Author
Dingyi Pan, Department of Engineering Mechanics, Zhejiang University, Hangzhou 310027, China
Email: dpan@zju.edu.cn.

I. Introduction

Inlets are designed to provide homogeneous, low-speed, high-pressure airflow to compressor entrance of aircraft engines over a wide range of flight conditions. Considering space limitation and stealth characteristic of aircrafts, short and highly offset S-duct inlets are always designed to maintain stability and performance. Owing to these, S-duct inlet is widely used in advanced aircrafts. Short diffusing S-duct inlets used for subsonic or high-subsonic aircraft engines, especially for turbojet engines, will be discussed and investigated here.

The short diffusing S-duct inlet always leads to complex aerodynamic characteristics, such as three-dimensional secondary flow and strong flow separation. In order to achieve stable and nearly uniform flow before the compressor entrance of the propulsion system, great endeavour has been devoted to improve the S-duct inlets performance since 1940s[1]. In early age, experiments acted as the major approach in S-duct inlet studies[2-5]. Wellborn[6] indicated that the duct curvature induced strong pressure driven secondary flows, and a large pair of counter-rotating vortices was captured in his S-duct inlet experiment. Recently, computational fluid dynamics (CFD) has been one of the most promising and practical methods for inlet design[7]. Berrier[8] predicted the reversal of pressure recovery trend by increasing inlet flux at both low and high Mach numbers and the CFD results were validated with experimental measurement. Besides, turbulence models used in S-duct inlets simulation were also thoroughly investigated, aiming to precisely simulate secondary flow and flow separation[9, 10].

The global performance of an inlet is significantly affected by its layout and geometry. Two of the key characteristics of inlet performance, i.e. the total pressure loss and the flow distortion, may vary a lot due to coupling effects of adverse pressure gradient and centrifugal force. Therefore, design optimization of the inlet is of great importance, and a well-designed inlet will enhance its global performance by reducing secondary flow and flow separation. Recently, optimization methods coupling with CFD simulation become a typical research approach in inlet design[11, 12]. Moreover, Zhang[13] used gappy proper orthogonal decomposition method in multidisciplinary design of a S-shaped intake. Hyo[14] developed a global optimization technique based on the stochastic kriging model and validated with Wellborn's[6] experiment.

Gan[15] conducted a three-dimensional diffusing S-duct inlet optimization, in which almost a hundred design cases were numerically studied.

All the design optimization in aforementioned studies only considered the inflow of inlet and neglected the outflow that influenced by lip and fore fuselage, which also plays an important role. Berrier[8] tested the boundary layer effects of different fore plates on the performance of S-duct inlets. Richard[16] investigated the aerodynamic characteristics of inlets with eight NACA 1-series lips and found that lip shape determined the inlet critical Mach number. Magnus[17] dealt with aerodynamic analysis of ducts including the effects of lips and fuselage interference, and indicated the inner flow in the diffuser were affected by fore fuselage boundary layer and local flow compression motivated by lip. Design and experiment of S-duct inlet with both inner and outer flow on a missile/aircraft were conducted by Li[18] and Xie[19], while both of them did not proceed to comprehensive optimization. Magnus[17] considered the lips and fuselage influence, while instead of optimization, only several ducts were designed and evaluated. Therefore, on one hand, the influence of outer flow should be taken into account in the design optimization of inlets. On the other hand, due to the complexity and computational cost for simulating both inner and outer flow, most of the optimizations did not consider the outer flow effect properly. For example, the numerical simulation of a typical integral inlet case with both inner and outer flow with 400 samples for optimization will cost one or two months on a computer of a four-core Intel processor with CPU speeds of 3.6GHz, which is unacceptable for engineering projects. Therefore, a comprehensive but also efficient model/approach is urgently needed to realize inlet optimization. In this paper, an optimization model/approach for S-duct inlets design is put forward, which will not only predict the influence of both inner and outer flow but also reduce the consuming time and computing resources in optimization system.

An S-duct scoop inlet used for high-subsonic aircrafts with Mach numbers range from 0.25 to 0.8 has been analysed. The designed Mach number is 0.7, in which condition the optimization model is conducted. Two of the most important coefficients, i.e., the total pressure recovery and the distortion, are

considered in the optimization system. Definition of total pressure recovery is σ=P_{T2} / P_{T0} . Pressure distortion describes the no uniform distribution of fluid, which affects the surge margin of an engine and indirectly influences the safety of an aircraft. Distortion criterion used here is *DC60* which is defined as:

$$DC60 = \left| \frac{\overline{P}_{Tm60} - \overline{p}_{Tm}}{\frac{1}{2}\overline{\rho}_a \overline{V}^2} \right|, \quad (1)$$

where $\overline{P}_{Tm60}$ is the minimum arithmetic mean total pressure within 60° fan section, and $\overline{p}_{Tm}$ is the arithmetic mean total pressure within 360° circumference section.

II. Integral model and efficient model for optimization

The total pressure loss and distortion of inlet is dominated by the diffuser flow, friction drag, lip separation and fore fuselage boundary layer. Friction drag is inevitable due to materials used, manufacturing technique as well as Mach number, altitude and surface area. Fore fuselage is always immutable when the aerodynamic layout of an aircraft is designed. As for lip section, NACA 1-series airfoil[16] (see List of ***Figures***

Figure 1) has been identified to possess a good performance on inlet lip design. The only adjustable factor for design optimization is diffuser shape. As a result, a simplified efficient model for S-duct inlet optimization based on diffuser shape change is developed, and its relationship with integral model is presented in Figure 2. The integral model covers both inner and outer flow in real circumstance, and efficient model is the diffuser only with inner flow, which will be conduct optimization on. The integral model's geometry profile and mesh should be divided into two parts, one for the outer flow and the other for the inner flow, as shown in Figure 3, because geometry and mesh of the efficient model will be exacted from corresponding integral model to guarantee identity.

The efficient model shares the same flight conditions, such as Mach number and flight height with the integral model. The outlet boundary conditions at the exit of inlet for both models are also consistent. Before optimization, flow field at the entrance of diffuser in integral model is solved, which will be

applied as the inlet boundary condition of efficient model in optimization process. The final optimized shape obtained from efficient model will be substituted into the integral model, so as to validate and analyse the optimal results.

III. Numerical methods

A. Numerical modelling and k–ω SST turbulence model

The short-offset S-duct inlets inherently have complex three-dimensional flows posing a challenge for CFD to accurately simulate the secondary flow and flow separation. The accuracy of CFD solutions mainly depends on the turbulence model employed. Different turbulence models have been applied to investigate the flow characteristics of S-duct, for example, k–ε turbulence model[8], lagged k–ω turbulence model[10], modified k–ω turbulence model[15]. Lee[20] compared the k-ω SST model with other two-equation turbulence models and pointed out that the result of k-ω SST model was better than the others. Zhang[13] also used k–ω SST turbulence model for S-duct numerical simulation and the results agreed well with experimental data. Fiola[9] compared the simulation results of diffusing S-duct using four different turbulence models, namely the Spalart–Allmaras, k-ε, k-ω SST, and Transition SST models. Fiola found k-ω SST turbulence model gave best agreement with the experimental data in predicting the pressure distribution along the duct, the separated flow region, and the secondary flow.

Ensure of accuracy and robustness, k–ω SST turbulence model is employed for the S-duct inlet simulation. k–ω SST model was implemented by Menter[21] to solve turbulence flow. k–ω SST model can account for the transport of the turbulent shear stress on the assumption that the principal turbulent shear-stress is proportional to the turbulent kinetic energy. It takes the turbulent boundary layer history effect into account by solving the complete transport equations of k and ω. Accordingly, the Reynolds Average Navier-Stokes equations are used as flow governing equations. The pressure-implicit based finite volume method and operators splitting algorithm for pressure-velocity coupling are utilized.

B. Boundary conditions

Figure 3 represents the geometric model considered and boundary conditions used. Since the geometric model is symmetrical, half model is simulated. For the integral model, the computational mesh that discretizes the domain has been divided into two parts, the outer zone and the inner region. Pressure-far-field boundary condition is chosen to initialize the simulation and outlet boundary condition at the exit of diffuser sets as pressure-outlet. Especially, the interface between outfield flow and inner flow should be reserved, so as to gain the pressure distribution at the entrance of diffuser. The diffuser wall, fore-plane/fuselage, lip and out cover are all with wall boundary condition.

For the efficient model, pressure-inlet boundary condition is utilized at the entrance of diffuser, which is obtained from the solution of corresponding integral model. The outlet boundary condition for efficient model keeps the same as the one of integral model.

C. Validations of current numerical simulation

In order to verify the reliability of numerical method used, the S-duct inlet A from previous work[22] has been investigated. The inlet A (Figure 4) is mounted on a flat plate surface so as to simulate the boundary layer created by fore fuselage. More details for the geometric parameters of inlet A can refer to literature[8] and report[22]. Total mesh number of the integral model used for simulation is 1.35 million, and a detailed study on the mesh independences of both integral model and efficient model will be presented in next subsection.

Compared the numerical simulation results with experimental data, the magnitudes of total pressure recovery under different Mach numbers are very close to each other, as shown in Figure 5. Within the calculated Mach number range, the total pressure recovery reduces as the Mach numbers increases, which is a typical phenomenon for most subsonic inlets. The circumferential total pressure distortion criterion, i.e., DPCPavg[22], for both CFD and experiment are exhibited in Figure 6. The simulation results for both total pressure recovery and distortion have good agreement with experimental data when Mach number is in range of 0.25~0.70, and the errors ($\epsilon = \frac{|f_{\mathrm{num}} - f_{\mathrm{exp}}|}{f_{\mathrm{exp}}}$) are less than 0.2% ($f = \sigma$) and 3% ($f = DPCPavg$), respectively. As Mach number increases to 0.8, the error increases to 0.3% for total pressure recovery and

15% for distortion. The error is mainly attributed to the severe and complex flow separation at high-subsonic condition.

Both the total pressure loss and distortion is expanding as Mach number increases, which is mainly subject to flow separation and secondary flow effect induced by improper inlet shape. Inlet design optimization is one of the most meaningful approaches to minimizing the total pressure loss and distortion.

D. Structured mesh and mesh independence validations

Mesh quality and quantity for numerical simulation is crucial especially in optimization, because less mesh number promotes the efficiency of optimization process. On the purpose of finding the most economic mesh numbers and ensuring the accuracy as well, four series of mesh are generated to validate the mesh independence. Total mesh numbers for integral model and corresponding efficient model are listed in Table 1. The size of the far-field calculating domain is 15 times of the inlet exit diameter. Structured meshes are generated for the S-duct inlet. Wall and entrance/exit cross-section domains are presented in Figure 7.

Table 1. Four types of mesh size

Mesh type	Integral model, million	Efficient model, million
Mesh-0	1.05	0.44
Mesh-1	1.35	0.66
Mesh-2	2.20	1.34
Mesh-3	4.00	2.67

Figure 8 shows the comparison of total pressure recovery distribution results with four types of mesh and experiment. The validation points coincide well with experiment for Mesh-1, Mesh-2 and Mesh-3.While Mesh-0 with the minimum mesh number predicts worse results than the other three. In order to cut down the calculating cost, the Mesh-1 with total mesh number of 1.35 million for integral model and 0.66 million for efficient model is chosen for the following design optimization.

IV. Framework of the design optimization system

The framework of design optimization system is displayed in Figure 9. We also choose the S-duct inlet A[22] as the prototype in the following optimization. The corresponding efficient model is exacted from the prototype. First, centreline shape and cross-section area are parameterized as the design variables for the efficient model. The Non-Uniform Rational B-Spline (NURBS) technique is used for shape construction. Structured meshes are automatically generated for each optimization sample. The k–ω SST model is applied in the simulation of the efficient model. The Non-dominated Sorting Genetic Algorithm II (NSGA-II) is utilized on the optimization model to get the optimal Pareto Front. The circulation will stop when the optimization goals is achieved. The last step is to transfer the optimal diffuser shape back to the S-duct inlet integral model and validate the final results.

A. Geometric parametrization design

Aerodynamic characteristic of S-duct inlets directly subjects to their geometric properties. Geometric parametrization is the first step for S-duct inlet design optimization. Wellborn et al.[6] used two equations to determine the centreline, which was defined by two planar circular arcs with identical radius. Berrier[22] defined the shape of the S-duct cross-section by super-ellipse shape equation. Other methods like Hicks-Henne functions[13] were used to formulate the variations of centreline, cross-section area and aspect ratio. Lee[23] utilized three analytical polynomial equations to describe the centreline and area distribution of diffusers. Polynomial equation can precisely describe uniform and continued changing rules. We apply quartic polynomial as the shape control equations for both centreline and cross-section area distribution.

Under certain disturbance, the boundary layer will transform from laminar flow to turbulence flow, i.e., boundary layer transition. Compared with turbulence flow, flow separation is easily induced in laminar flow. Strategies such as suction device and transition tape are employed to control the transition process in advance before the entrance of inlet. Appropriate centreline and cross-section area distribution design of inlet is also able to effectively prevent laminar flow separation by decreasing adverse pressure gradient.

Centreline distribution determines the transverse pressure gradient which results in secondary flow. Affected by inertial force, the distribution of inner flow field in the S-duct inlet is uneven leading to serious flow distortion. Proper centreline design is crucial in eliminating secondary flow and distortion. The cross-section area distribution determines the expansion ratio of inlet, which will affect the aerodynamic performance. Both centreline and area distribution will be uniformly given by the same mathematical representation:

$$\overline{\mathrm{Y}}_i = \mathrm{f}(\overline{x}_i),\ (\overline{x}_i = \mathrm{x}_i / L, \mathrm{i} = 1,2,3,\ldots N)\ , \tag{2}$$

$$\mathrm{f}(\overline{x}_i) = A' \times \overline{x}_i^{\,4} + B' \times \overline{x}_i^{\,3} + C' \times \overline{x}_i^{\,2} + D' \times \overline{x}_i + E'\ . \tag{3}$$

For centreline, dimensionless parameters $\overline{Y}_i = y_i / H$. And for cross-section area, $\overline{Y}_i$ is the relative growth rate which is defined as $\overline{Y}_i = (A_i - A_1)/(A_2 - A_1)$. Letters A', B', C', D', E' represent the shape adjustment factors. The shape of the diffuser is shown in Figure 10.

Under the limitation of engine and fuselage frame, shape control function will be subject to some constraints, which will dismiss lots of inapplicable shapes. Here the design constraints for both centreline and cross are as following:

$$\begin{cases} \overline{\mathrm{x}}_i \in [0,1], \overline{Y}_i \in [0,1] \\ \overline{Y}_1 = 0, \overline{Y}_N = 1 \\ \overline{Y}_1{}' = 0, \overline{Y}_N{}' = 0 \end{cases}. \tag{4}$$

Solution of equation (4) is

$$D' = E' = 0, \begin{cases} C' \in [0,6] \\ B' = 4 - 2C' \\ A' = C' - 3 \end{cases}. \tag{5}$$

The cross-section shape is composed of up half circle and down half ellipse, which makes it easy to construct the area of cross-section. Non-dimensional centreline shape and cross-section area trend lines with different adjustment factors (A'=0, 1, 2, 3, 4, 5, 6) are illustrated in Figure 11.

For an S-duct inlet, the shorter length the worse pressure recovery. A shorter S-duct corresponds to a more rapidly change of shape curvature, which may easily lead to flow distortion and secondary flows. On the other hand, the inlet length is always constrained considering the whole aircraft frame and the

aerodynamic drag, therefore special design and optimization should be conducted on short diffusing S-duct inlet to achieve relatively high pressure recovery. Under the constraints of the fuselage frame, and engine performance, some general parameters of inlet such as length, offset, area ratio of diffuser and exit area are fixed in the design, as specified in Table 2. All the length parameters are normalized by the diameter of diffuser's exit.

Table 2. Values of fixed Geometric Parameters of the S-duct inlet

Variable	value	Unit
D_2	0.0622	m
A_2	0.003037	m^2
L/D_2	3.144	
H/D_2	0.893	
Area ratio	1.07	

B. The NURBS geometry representation technique

The shape of efficient model in the optimization process is automatically represented by NURBS technique[24]. Given the ordered knot vector $E=\{\xi_1, \xi_2,\ldots\xi_i,\ldots, \xi_{n+p+1}\}$, where ξ_i are the knot nodes, p is the degree and n is the number of basis function. Then the i^{th} B spline basic function is defined as:

$$N_{i,0}(\xi)=\begin{cases}1 & (\xi_i \le \xi \le \xi_{i+1})\\ 0 & \text{others}\end{cases}, \tag{6}$$

$$N_{i,p}(\xi)=\frac{\xi-\xi_i}{\xi_{i+p}-\xi_i}N_{i,p-1}(\xi)+\frac{\xi_{i+p+1}-\xi}{\xi_{i+p+1}-\xi_{i+1}}N_{i+1,p-1}(\xi). \tag{7}$$

Basic function of NURBS surface is composed of two spline basic functions N and M:

$$R_{ij}^{w}(\xi,\eta)=\frac{N_{i,p}(\xi)M_{j,p}(\eta)\omega_{ij}}{\sum_{i=1}^{n}\sum_{j=1}^{m}N_{i,p}(\xi)M_{j,q}(\eta)\omega_{ij}}, \tag{8}$$

where ω_i are weight coefficients. Then NURBS surface is in the form:

$$S^{w}(\xi,\eta)=\sum_{i=1}^{n}\sum_{j=1}^{m}R_{ij}^{w}(\xi,\eta)B_{ij}^{w}. \tag{9}$$

The precision of NURBS geometry representation is subject to the control point number and p degree. Refinement of control points will increase precision of surface building. In the S-duct representation, ξ is along the centreline direction and η is at the cross section which is normal to the centreline. The NURBS

control point number for the efficient optimization model is 50*24. Three degrees (p=3) in both ξ and η direction are chosen to retain the second order continuity of S-duct.

C. NSGA-II and Pareto Front

NSGA-II is always applied for solving multi-objective problems because of its high efficiency, fast convergence, good fitness properties and uniformly distributed Pareto Front[25]. A pareto front is the set of design parameterizations that are all Pareto efficient, where each design has the "optimal" combination of objective values and improving one objective is impossible without sacrificing one or more of the other objectives. Pareto front helps a designer to make tradeoffs within this set of design parameters to obtain the optimal solutions. In NSGA-II, each objective parameter is treated separately and a pareto front is constructed by selecting feasible non-dominated designs. NSGA-II is well-suited for highly non-linear and discontinuous design spaces. Standard genetic operation of mutation and crossover are performed on the designs. NSGA-II utilizes fast non-dominated sorting technology to decrease the computation complexity and based on elitist mechanism to improve accuracy.

The procedure of NSNA-II is simply introduced below and demonstrated in Figure 12. First, it randomly generates the father generation P_t which has the size of N. Based on the father generation, the son generation Q_t is created with the same size. Then both P_t and Q_t are combined to the population R_t with the size of 2N. Use the non-dominated sorting method on R_t to ensure the elitism. Secondly, it defines F_1, F_2, F_3 as the best, the second and the third solutions of population R_t, respectively. If F_1 is smaller than N, then put all members of F_1 into the next generation P_{t+1}. The remaining of P_{t+1} will be selected from F_2, F_3 according to their sorting. The P_{t+1} generation should reach size of N based on crowded-comparison selection criterion. The same mechanism should be conducted to produce the next generation until enough number of Pareto Front is found. In the S-duct inlet optimization process,

population size N sets as 20, and 20 generations have been carried out to obtain the last Pareto Front (see Figure 13).

V. Result analysis and discussion

A. Optimized shape of S-duct inlet

A suggested optimal design is chosen from the Pareto Front obtained from the optimization results (see Figure 13). The geometry parameters of suggested optimal S-duct shape are displayed in Figure 14. Subfigure a) and b) are the comparison of non-dimensional centreline shape and cross-section area distribution for original and optimal inlets, respectively. The gradient of the optimal shape is more uniform and gentle than the original shape's. Subfigure c) is the non-dimensional radius distribution for up half circle and d) is the non-dimensional Semi minor axis distribution of down half ellipse at cross section.

B. Validation for efficient optimization model

The optimal diffuser shape obtained by efficient model is feedback to the integral model for validation. Table 3 gives the specific results of original and optimized efficient/integral models at designed Mach number (Ma=0.7). As indicated in Table 3, the efficient model predicts that the optimal inlet's total pressure recovery has been increased by 0.38% and *DC60* has been decreased by 0.0481. With the corresponding integral model, the total pressure recovery has been increased by 0.40% and *DC60* has been decreased by 0.0477. The prediction for both total pressure recovery and distortion of efficient model agrees well with the exact integral model.

It should be noted that the pressure boundary condition at the inlet of efficient model is fixed as a constant during optimization. To confirm this, we extract the pressure at the entrance of diffuser from the optimized integral model, and the average pressure is almost same with the one of the original integral model. Therefore, the effect of diffuser shape change on the inlet pressure is negligible.

Figure 15 and Figure 16 respectively present the total pressure recovery and distortion distribution at different Mach numbers for original and optimized models. The dashed lines are the results of efficient

model, and the solid lines are those of the corresponding integral model. Both figures validate that the simplified model can be used as a substitution for S-duct inlet when conducting design optimization. The time cost has been cut by 70% for the optimization project in current work.

Table 3. Comparison of results of original and optimized model (Ma=0.7).

results	Efficient model		Integral model	
	σ	*DC60*	σ	*DC60*
original	97.05%	0.2138	97.01%	0.2195
optimized	97.43%	0.1657	97.41%	0.1718
Increased value	0.38%	-0.0481	0.40%	-0.0477

Figure 17 demonstrates the specific total pressure contour at the symmetry plane at Ma=0.7 with altitude of 100m, where four low pressure areas (A, B, C, and D) are marked. Comparison of subfigure a) and b) illustrates the low-pressure district B and D predicted by efficient model trends to be identical with the real distribution in integral model. While district A and C in subfigure a) and b) seem to be a little different. However, the maximum deviation of DC60 for efficient model from integral model is about 0.006 at Mach number 0.7, which is much smaller than the difference (0.048) between optimized results and original results. The total pressure recovery deviation is only 0.02% (Ma= 0.7) which is negligible and acceptable from the viewpoint of engineering application.

C. Analysis of optimization results

As indicated in Figure 15 and Figure 16, results of optimized shape are compared with original ones. For the total pressure recovery (see Figure 15), the effect of optimization is magnifying as the increasing of Mach numbers. At Ma=0.25~0.5, the total pressure recovery stays almost the same with the original ones. Because the pressure loss caused by shape is nearly 0 at small Mach numbers, and the only 1% loss is mainly induced by friction. When Mach number increases to 0.6 or larger, the benefit from optimization becomes much more distinct. For total pressure distortion (see Figure 16), the superiority of optimized shape is obvious at all Mach numbers. Compared with the original S-duct inlet, the average reduction of *DC60* for all cases is 0.0433.

Compared subfigure b) with c) in Figure 17, all the four low pressure areas are obviously shrunk by optimization. Streamlines at the exit cross-section, as shown in Figure 18, indicate that the secondary flow and vortex intensity at crosswise is effectively reduced after optimization. Total pressure recovery contour maps at the exit of inlet with Mach numbers range 0.25~0.7 are illustrated in Figure 19 (under different α) and Figure 20 (β=6). In Figure 19, the total pressure recovery of each right half circle (optimized inlet) is better than the corresponding left one (original inlet). All the results comparison in Figure 17-19 demonstrates that the suggested optimized shape efficaciously restricts the expanding of low energy flow and keeps relatively high total pressure recovery even under large angles of attack or sideslip.

VI. Summery

A fast multi-objective design optimization method for scooped S-duct inlets with both inflow and outflow is developed and validated. A simplified efficient method has been developed in the optimization system to reduce the computing resources. The numerical simulation method is based on k–ω SST turbulence model, which has been validated and the results agree well with the experiment. An optimization system based on NSGA-II is built and NURBS technique is applied on shape representation. The efficient method has been validated to be reliable and through which the time cost has been reduced by 70% in the optimization procedure.

Compared with original inlet, the total pressure recovery of optimized inlet has increased from 97% to 97.4%, and the total pressure distortion *DC60* has been decreased by 0.0477 (21.7% of origin) at design Mach number. For total pressure recovery, the effect of optimization is magnified as the increase of Mach numbers. While for total pressure distortion, it is obviously cut down at all the calculated Mach numbers. Besides, inlet performance deteriorates as the increasing of angle of attack or sideslip, while optimization is able to restrict the enlargement of low energy flow and secondary flow.

The design optimization method introduced here can be applied to other inlets, such as top-mounted S-duct inlet, diverterless supersonic inlet (DSI), baffle inlet and so forth. In addition, the boundary layer of S-duct inlet which contains low-energy flow plays an important role in reducing aerodynamic

performance. Boundary layer control measures might be taken to improve the overall inlet performance. The future work might combine the optimization method described above with the boundary layer and flow control measures.

Moreover, the optimization objectives in this paper are total pressure recovery and distortion, both of which are related to aerodynamic characteristics. While expect for aerodynamic performance, electromagnetic property should also be considered especially for stealth aircrafts. Under this circumstance, multi-objective optimization method and multidisciplinary design should be combined to investigate on both the aerodynamic and electromagnetic performance of inlets in the near future.

Declaration of Conflicting Interests

The authors declared no potential conflicts of interest with respect to the research, authorship, and/or publication of this article.

Acknowledgments

The authors would like to acknowledge the support provided by Zhejiang Provincial Natural Science Foundations (LY18A020002, LQ18E090010).

References

1. Weske JR. Pressure loss in ducts with compound elbows. *Technical Report Archive & Image Library*. 1943.
2. Syberg J, Koncsek J and Surber L. Performance variations in high aspect ratio subsonic diffusers due to geometric constraints in supersonic tactical aircraft inlet installations. In: *AIAA/SAE/ASME 16th Joint Propulsion Conference*. Hartford, Connecticut, USA, 30 June-2 July 1980, AIAA-80-1106.
3. Little BH and Trimbol WS. An experimental investigation of S-duct diffusers for high-speed prop-Fans. In: *AIAA/SAE/ASME 18th Joint Propulsion Conference*, Cleveland, Ohio, USA, 21-23 June 1982, AIAA-82-1123.

4. Ball WH. Experimental investigation of the effects of wall suction and blowing on the performance of highly offset diffusers. In: *AIAA/SAE/ASME 19th Joint Propulsion Conference*, Seattle, Washington, USA, 27-29 June 1983, AIAA-83-1169.

5. Kitchen RA and Sedlock D. Subsonic diffuser development of advanced tactical aircraft. In: *AIAA/SAE/ASME 19th Joint Propulsion Conference,* Seattle, Washington, USA, 27-29 June 1983*,* AIAA-83-1168.

6. Wellborn SR, Reichert BA and Okiishi TH. An experimental investigation of the flow in a diffusing S-duct. In: *AIAA/SAE/ASME 28th Joint Propulsion Conference and Exhibit*, Nashville, Tennessee, USA, 6-8 July 1992, AIAA-92-3622.

7. Goldsmith EL and Seddon J. *Practical intake aerodynamic design*, AIAA Education Series, AIAA, Washington, DC, 1993.

8. Berrier BL and Allan BG. Experimental and Computational Evaluation of Flush-Mounted, S-Duct Inlets. In: *42nd AIAA Aerospace Sciences Meeting and Exhibit*, AIAA 2004-764, Reno, Nevada, USA, 5-8 January 2004, AIAA -2004-764.

9. Fiola C and Agarwal RK. Simulation of Secondary and Separated Flow in a Diffusing S-Duct using four different turbulence models. *Proc IMechE, Part G: J Aerospace Engineering* 2014; 228:1954-1963.

10. Xiao Q, Tsai H and Liu F. Computation of Transonic Diffuser Flows by a Lagged k-ω Turbulence Model. *J Propul Power* 2003;19:473-483.

11. Lefantzi S and Knight DD. Automated Design Optimization of a Three-Dimensional S-Shaped Subsonic Diffuser. *J Propul Power* 2002; 18:913-921.

12. Zhang WL, Knight DD and Smith D. Automated design of a three dimensional subsonic diffuser. *J Propul Power* 2000; 16: 1132-1140.

13. Zhang JM, Wang CF and Lum KY. Multidisciplinary Design of S-Shaped Intake. In: *26th AIAA Applied Aerodynamics Conference*, Honolulu, Hawaii, USA, 18-21 August 2008, AIAA- 2008-7060.

14. Hyo GB, Soo HP, Jank HK, et al. Efficient Global Optimization for S-duct Diffuser Shape Design. *Proc IMechE, Part G: J Aerospace Engineering* 2013;227:1516-1532.

15. Gan WB and Zhang XC. Design optimization of a three-dimensional diffusing S-duct using a modified SST turbulent model. *Aerosp Sci Technol* 2017; 63: 63-72.

16. Richard RJ. An investigation of several NACA 1-series inlets at Mach numbers from 0.4 to 1.29 for mass flow ratios near 1.0. NASA TM X-3324, 1975.

17. Magnus T. Design and Analysis of Compact UAV Ducts. In: *24th AIAA Applied Aerodynamics Conference*, San Francisco, California,USA,5-8 June 2006,AIAA-2006-2828.

18. Li Q, Guo R and Fu Q. Design and performance of S-shaped inlet for high subsonic missiles. *J Nanjing Univ Aeronaut Astronaut* 2002; 34:108-113.

19. Xie W and Guo R. Flow Field of Ventral Diverterless High Offset S-shaped Inlet at Transonic Speeds. *Acta Aeronaut Astronaut Sin* 2008;2:207–214.

20. Lee BJ and Kim C. Automated design methodology of turbulent internal flow using discrete adjoint formulation. *Aerosp Sci Technol* 2007;11:163-173.

21. Menter FR. Zonal Two Equation k-ω Turbulence Models For Aerodynamic Flows. In: *24th Fluid Dynamics Conference*, Orlando, Florida, USA,6-9 July 1993, AIAA -93-2906.

22. Berrier BL, Carter MB and Allan BG. High Reynolds Number Investigation of a Flush-Mounted, S-Duct Inlet With Large Amounts of Boundary Layer Ingestion. NASA/TP-2005-213766. 2005.

23. Lee CC and Boedicker C. Subsonic diffuser design and performance for advanced fighter aircraft. In: *AIAA/ AHS /ASEE Aircraft Design Systems and Operations Meeting,* Colorado Springs, Colorado, USA, 14-16 October 1985*,* AIAA-85-3073.

24. Piegl L and Tiller W. *The Nurbs Book(Monographs in Visual Communication*), 2nd ed., Springer, Berlin, 1997.

25. Deb KD, Pratap A, Agarwal S, et al. A fast and elitist multiobjective genetic algorithm: NSGA-II. *IEEE Transactions on Evolutionary Computation* 2002; 6:182-197.

Appendix

Nomenclature

A	cross-section area, m^2
A_1	entrance area of the diffuser, m^2
A_2	outlet area of the diffuser, m^2
AR	aspect ratio
b	semi-minor axis of down half ellipse cross-section, m
B_i	the control knot
D_2	outlet diameter of the diffuser, m
$DC60$	total pressure distortion criterion
$E(\xi)$	knot vector
F	solutions of population R_t
H	the offset distance, m
L	the length of inlet, m

Ma	Mach number
N	total number of shape control points
$N(\xi)$	B-spline basic function
n	number of basis function
p	degree of B-spline
P_{t}	father generation
P_{t+1}	optimized next generation
P_{T0}	free-stream total pressure, Pa
P_{T1}	average total pressure of the diffuser entrance plane, Pa
P_{T2}	average total pressure of the diffuser exit plane, Pa
$\overline{p}_{Tm}$	arithmetic mean total pressure within 360°circumference section, Pa
$\overline{P}_{Tm60}$	the minimum arithmetic mean total pressure within 60° fan section, Pa
Q_t	son generation
R	radius of cross-section up half circle, m
R_{ij}^{w}	NURBS surface basic function
R_t	combined population
S^{w}	NURBS surface function
V	average velocity at the measured cross-section, m/s
x_i	the horizontal coordinates at the control point i along the centreline, m
y_i	the vertical coordinates at the control point i along the centreline, m
$\overline{Y}_i$	shape dimensionless parameters
$\overline{Y}_i'$	derivative of shape dimensionless parameters
α	angle of attack, degree (°).
β	angle of sideslip, degree (°).
ξ_{i}	knot nodes

$\overline{\rho}_a$	average density of the measured cross-section, kg/m^3
σ	the total pressure recovery
ω_i	weight coefficient

List of Figures

Figure 20. Total pressure recovery contour maps at the exit of inlet when β=6°. a) Original inlet β=6°, b) Optimized inlet β=6°.

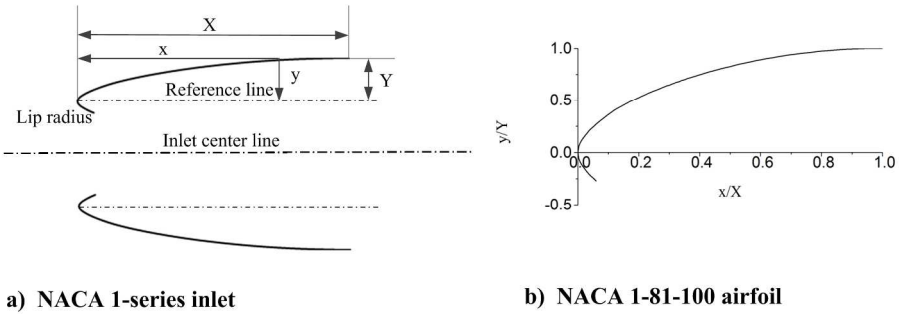

a) NACA 1-series inlet **b) NACA 1-81-100 airfoil**

Figure 1. NACA 1-series inlet design and sample airfoil, a) NACA 1-series inlet, b) NACA 1-81-100 airfoil.

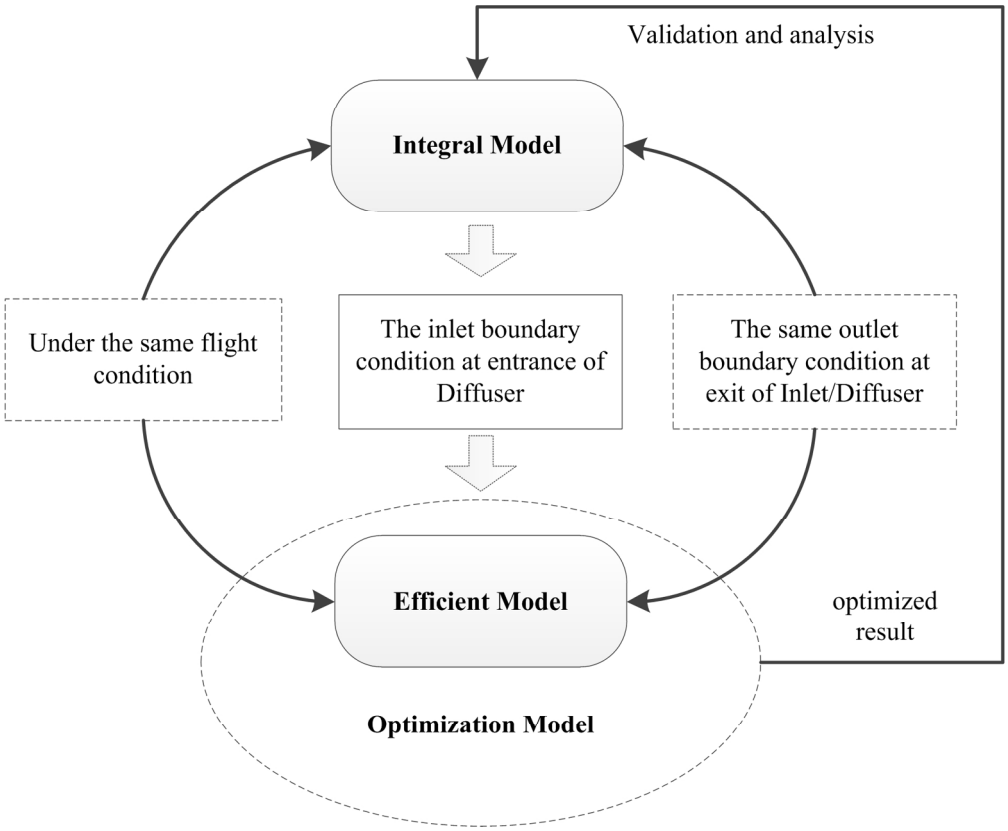

Figure 2. The efficient optimization model for S-duct inlet.

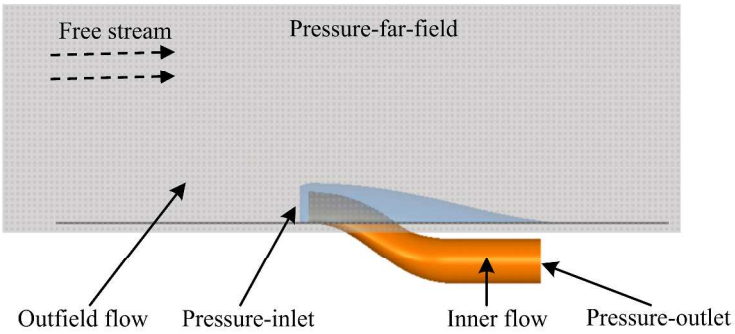

Figure 3. Geometry model and boundary conditions.

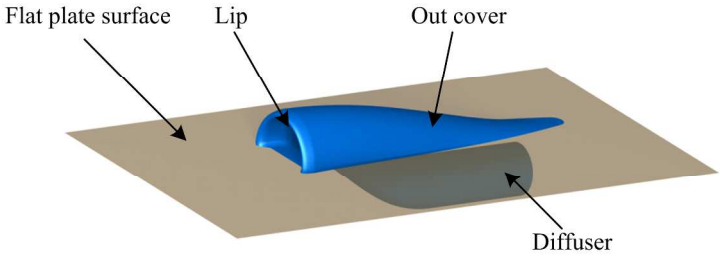

Figure 4. Three-dimensional model for the S-duct inlet A

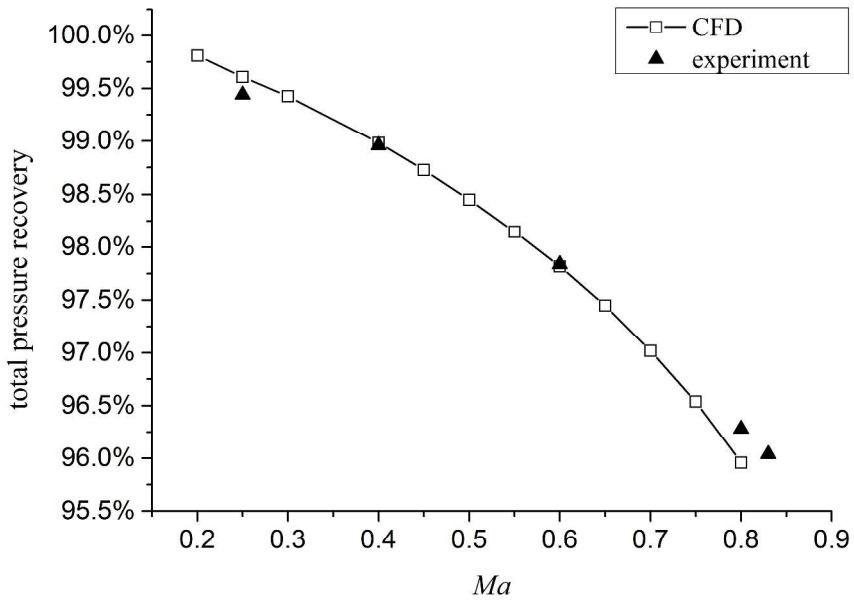

Figure 5. Total pressure recovery comparison of numerical simulation and experiment8

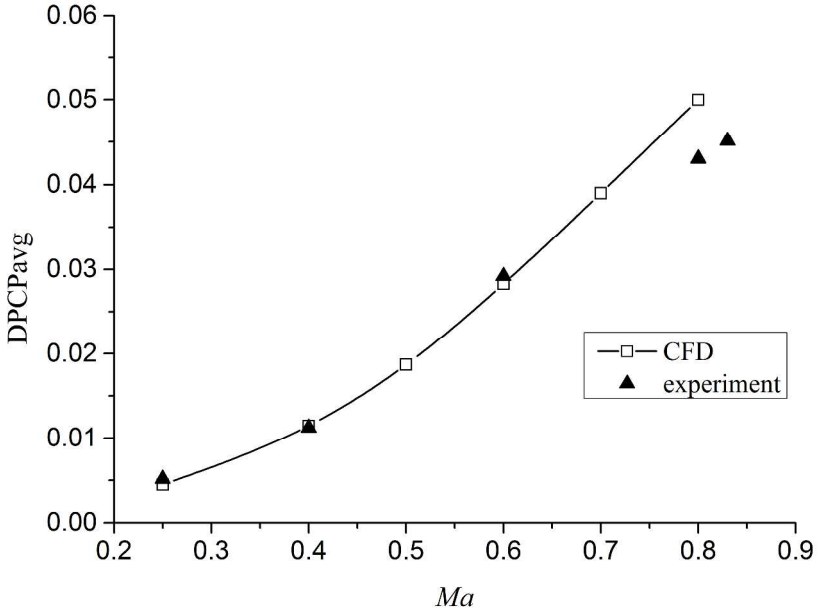

Figure 6. Total pressure distortion comparison of numerical simulation and experiment8

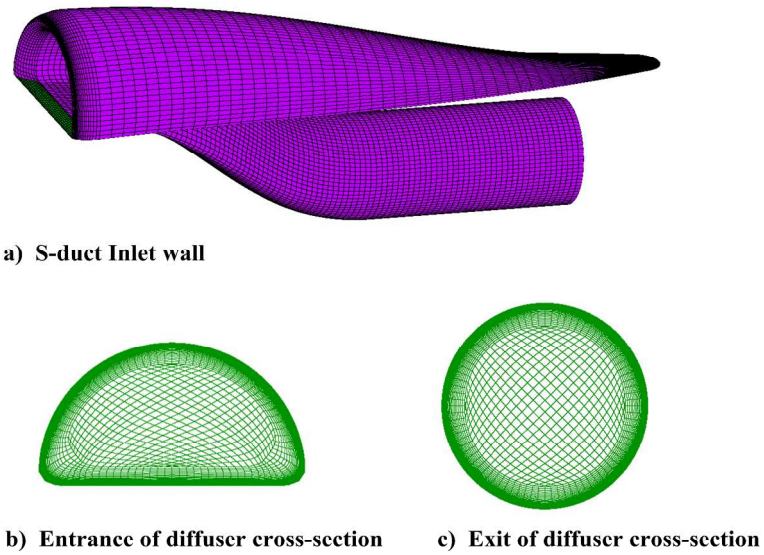

Figure 7. Structured girds domain for S-duct inlet. a) S-duct Inlet wall, b) Entrance of diffuser cross-section and c) Exit of diffuser cross-section.

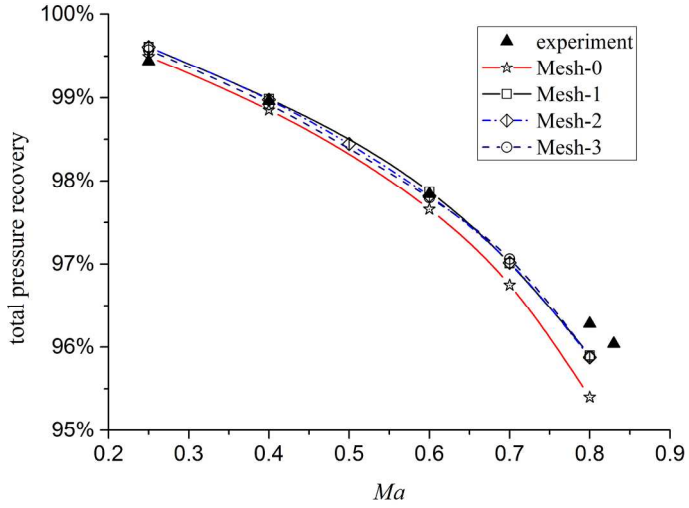

a) Integral model

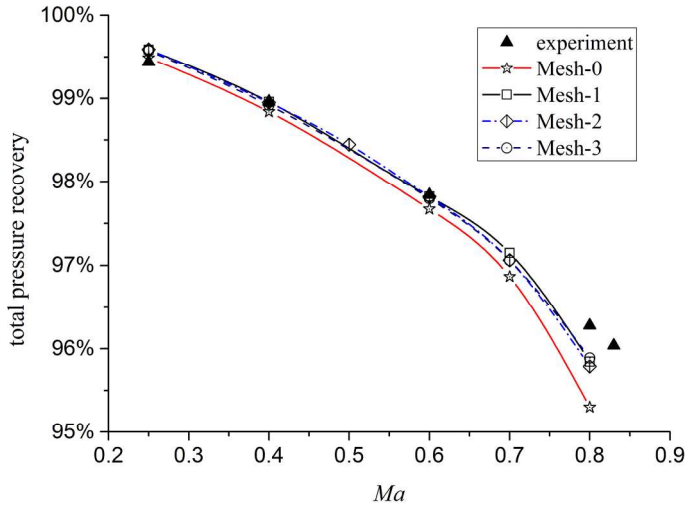

b) Efficient model

Figure 8. Total pressure recovery distribution of different mesh size. a) Integral model, b) Efficient model.

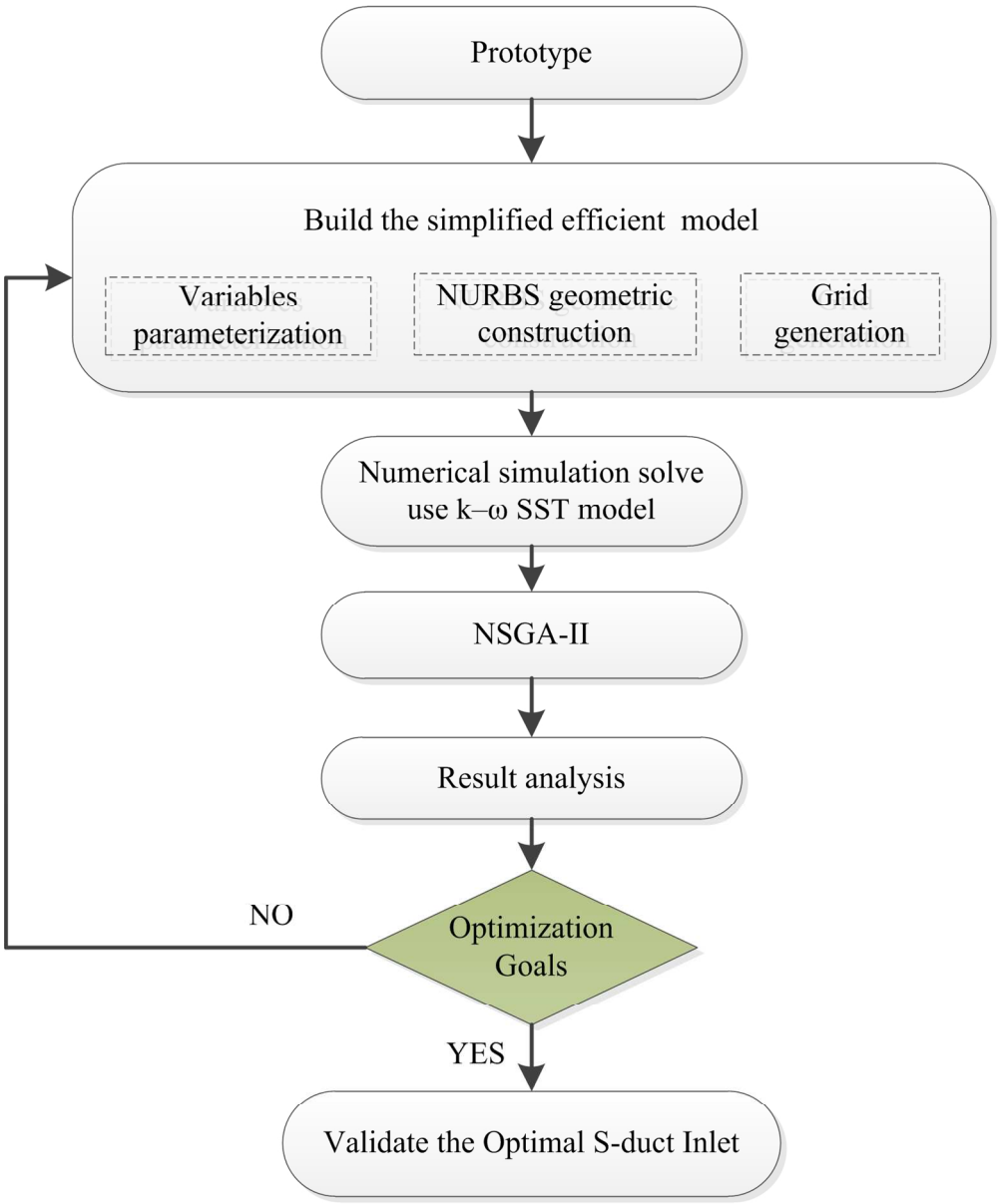

Figure 9. Framework of design optimization system.

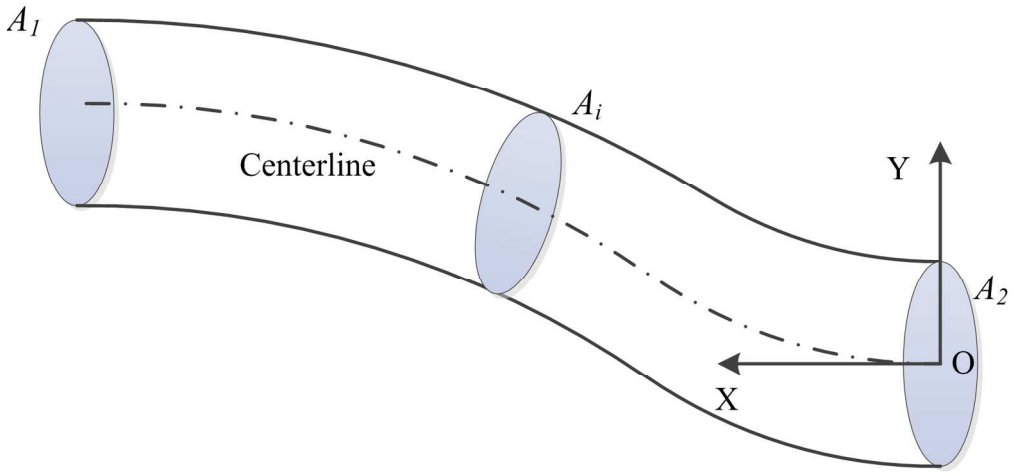

Figure 10. Baseline of the diffuser for S-duct inlet

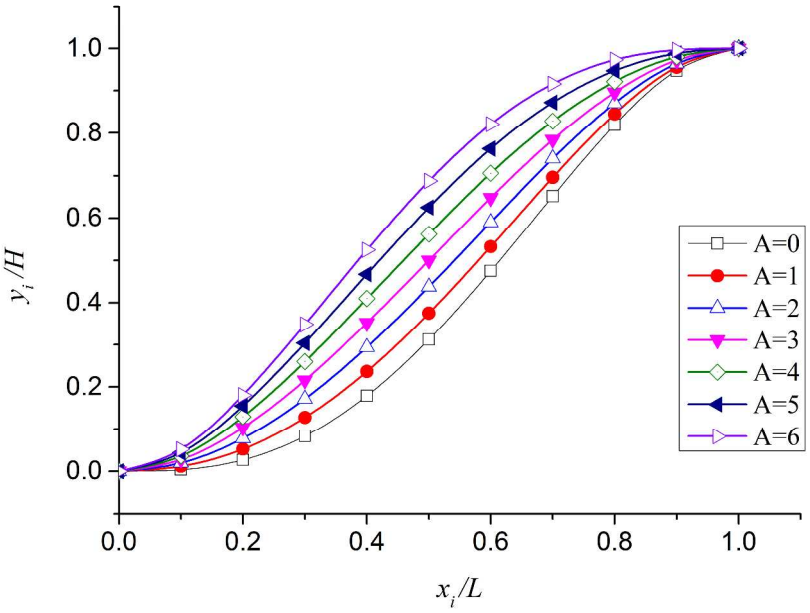

Figure 11. Shape trend line at different adjustment factors.

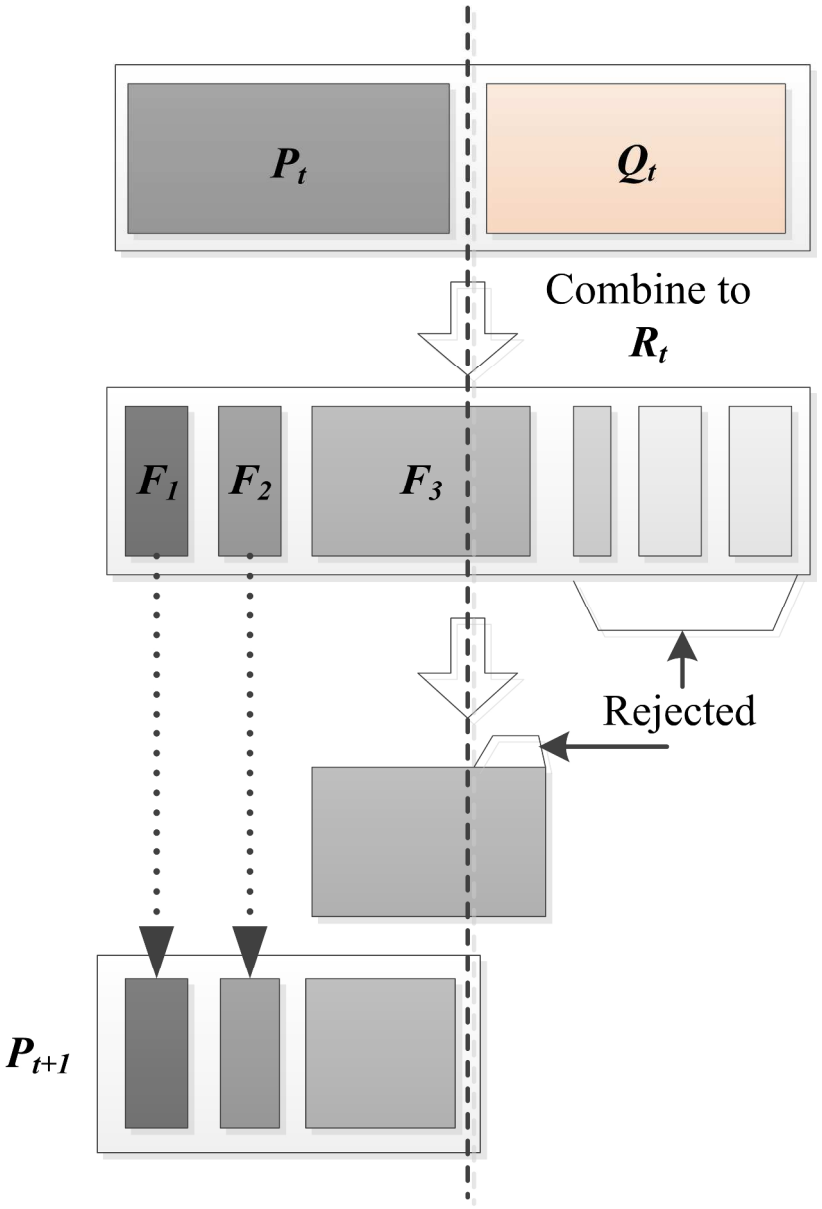

Figure 12. NSGA-II simplified procedure.

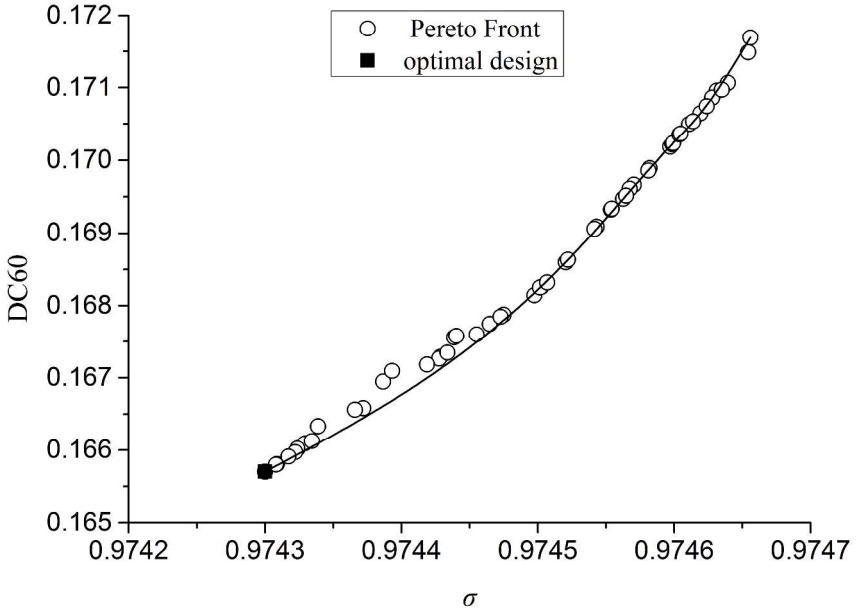

Figure 13. Pareto Front of optimization.

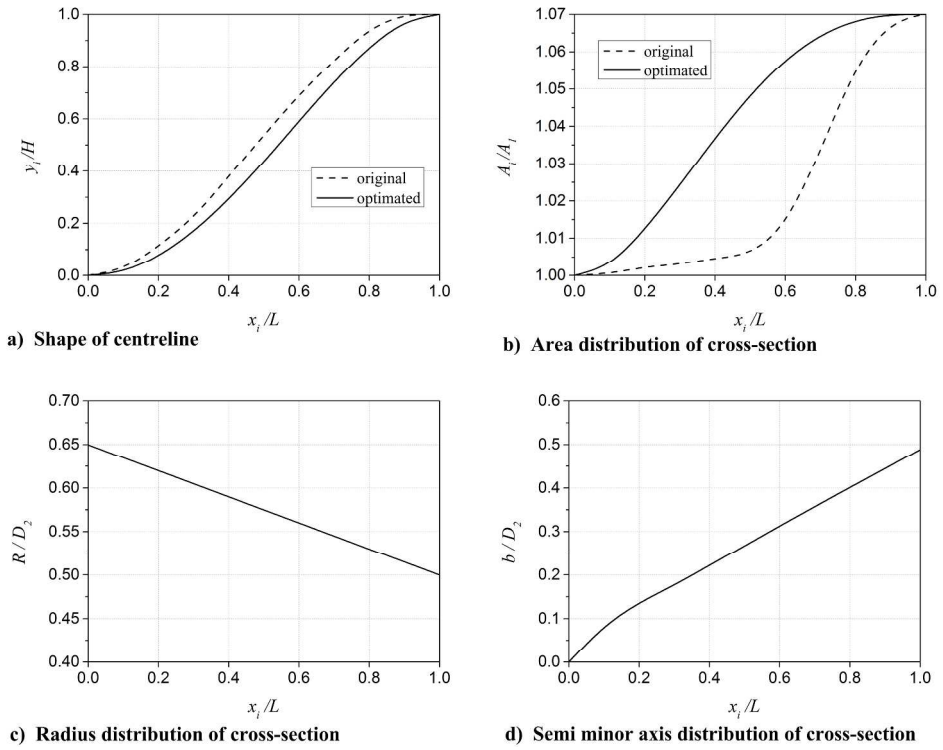

Figure 14. Geometry parameters of suggested optimal diffuser. a) Shape of centreline, b) Area distribution of cross-section, c) Radius distribution of cross-section and d) Semi minor axis distribution of cross-section.

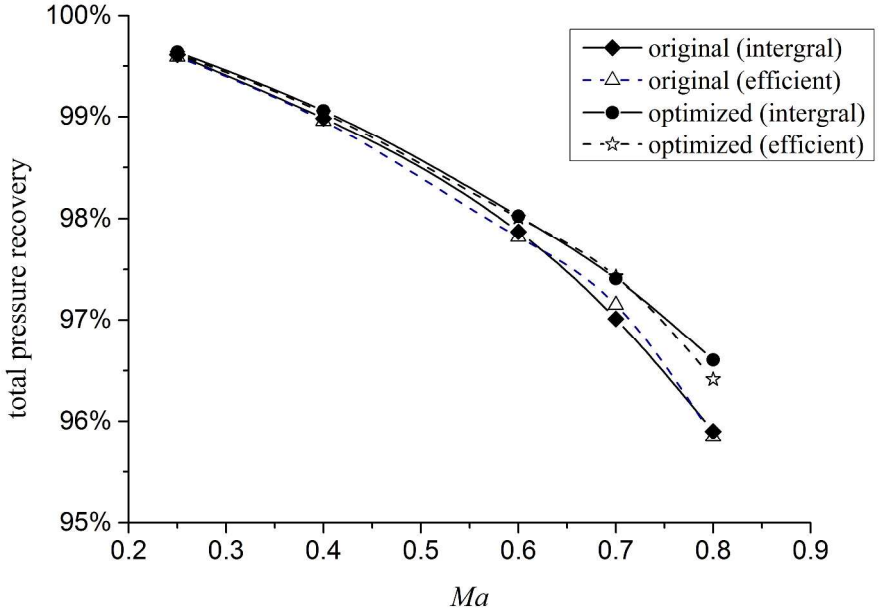

Figure 15. Total pressure recovery distribution at different Mach numbers.

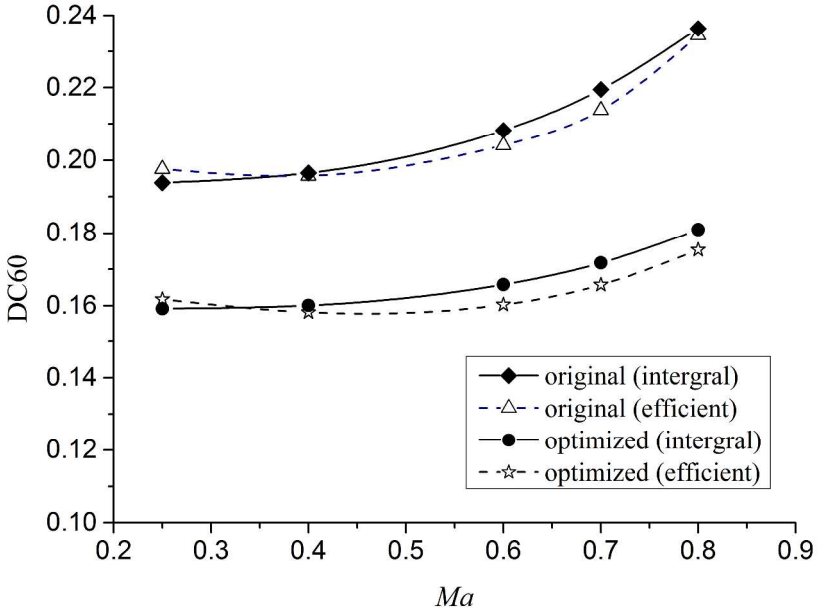

Figure 16. Total pressure distortion distribution at different Mach numbers.

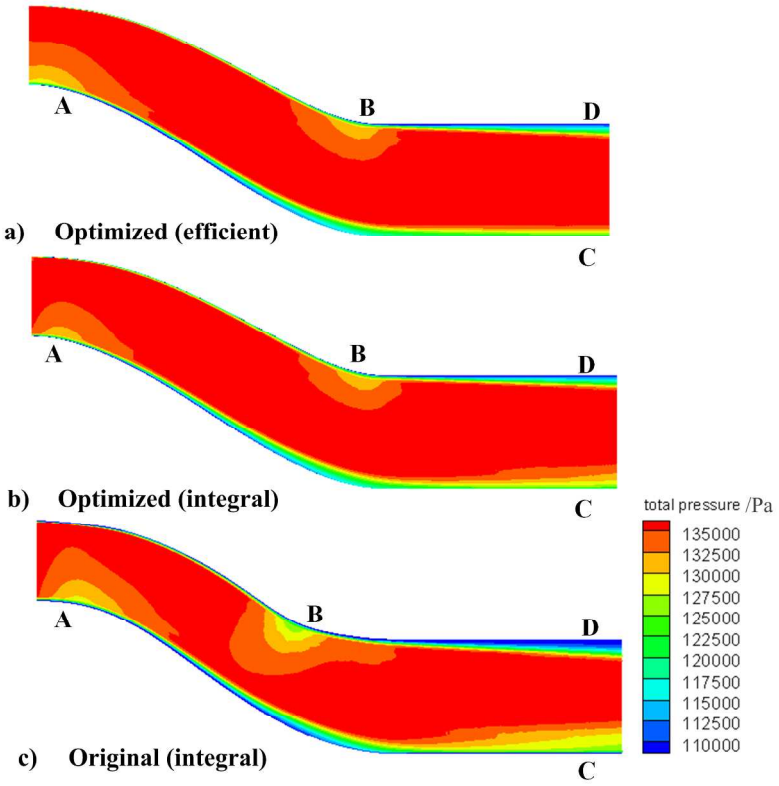

Figure 17. Total pressure contour maps at symmetry plane (Ma=0.7).

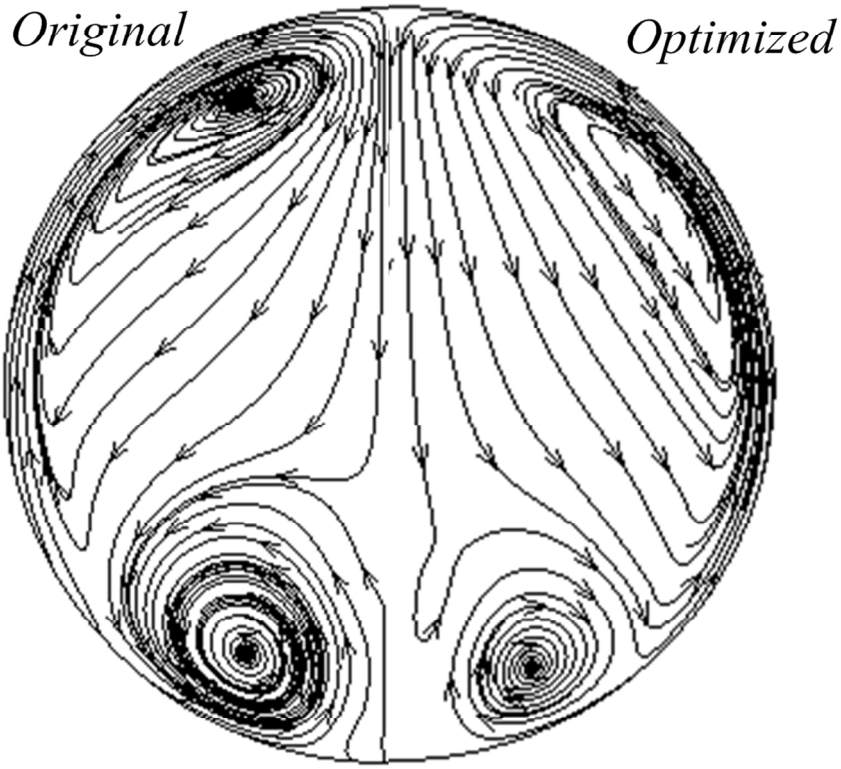

Figure 18. Streamline at the exit of origin and optimized S-duct inlet (Ma=0.7).

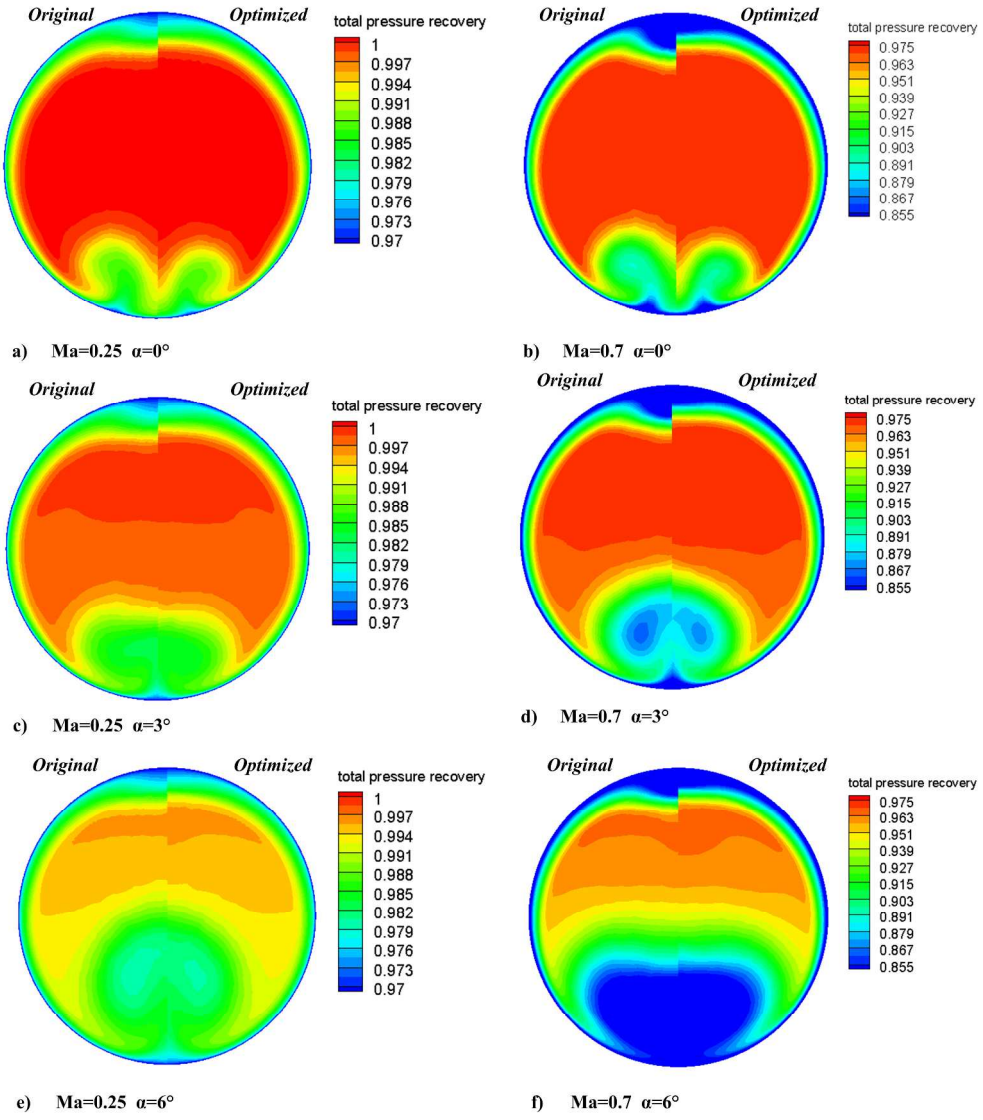

Figure 19. Total pressure recovery contour maps at the exit of inlet. a) Ma=0.25, α=0°, b) Ma=0.7, α=0°, b) Ma=0.25, α=3°, c) Ma=0.7, α=3°, d) Ma=0.25, α=6° and e) Ma=0.7, α=6°.

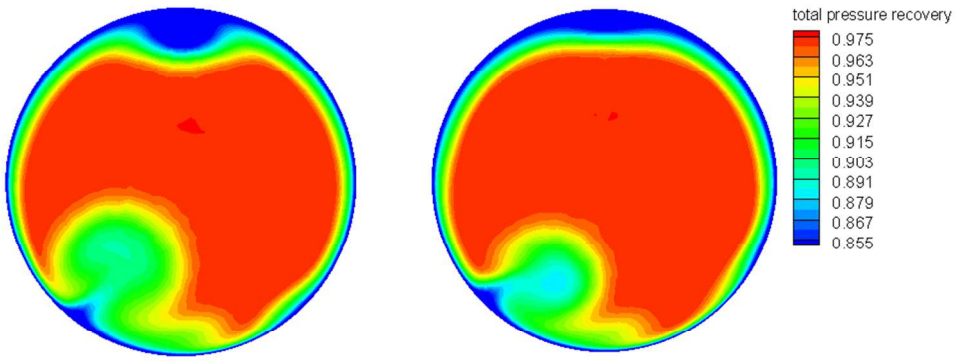

a) Original inlet β=6° **b) Optimized inlet β=6°**

Figure 20.Total pressure recovery contour maps at the exit of inlet when β=6°. a) Original inlet β=6°, b) Optimized inlet β=6°.